

Magnetic structures of $M\text{Fe}_{4+\delta}\text{Al}_{8-\delta}$ ($M=\text{Lu},\text{Y}$)

J. A. Paixão and M. Ramos Silva

Departamento de Física, Faculdade Ciências e Tecnologia, Universidade de Coimbra, P-3004-516 Coimbra, Portugal

J. C. Waerenborgh and A. P. Gonçalves

Instituto Tecnológico e Nuclear, P-2686-953 Sacavém, Portugal

G. H. Lander

European Commission, Joint Research Centre, Institute for Transuranium Elements, Postfach 2340, D-76125 Karlsruhe, Germany

P. J. Brown

Institut Laue-Langevin, 156X, F-38054 Grenoble Cedex, France

M. Godinho

Departamento de Física, Faculdade de Ciência, Universidade de Lisboa, P-1749-016 Lisboa, Portugal

P. Burllet

Département de Recherche Fondamentale sur la Matière Condensée, Commissariat à l'Énergie Atomique-Grenoble, F-38054 Grenoble, France

(Received 18 July 2000; published 4 January 2001)

The magnetic structure of nonstoichiometric $\text{LuFe}_{4+\delta}\text{Al}_{8-\delta}$ and $\text{YFe}_{4+\delta}\text{Al}_{8-\delta}$ compounds with a small Fe excess ($\delta \sim 0.40$) was investigated by Mössbauer spectroscopy, magnetization measurements, and both polarized and unpolarized neutron-scattering experiments on single crystals. The small excess of Fe atoms substitute Al at the $8j$ positions and have a pronounced effect on the magnetic properties. The Néel temperature decreases from ~ 190 to 100 K and the magnetic ordering changes from the cycloid modulation found in the stoichiometric compounds to an amplitude modulated wave with a much shorter period.

DOI: 10.1103/PhysRevB.63.054410

PACS number(s): 75.25.+z

I. INTRODUCTION

The $M\text{Fe}_4\text{Al}_8$ (M =rare earth or actinide) family of ternary intermetallic compounds with the ThMn_{12} type of structure show unusual magnetic properties which have been the subject of considerable controversy for quite some time.¹

These compounds crystallize in a body centered tetragonal cell, space group $I4/mmm$. The rare earth occupies the $2a$ crystallographic sites, at the origin and center of the cell. The remaining atoms occupy the $8f$, $8i$, and $8j$ sites, with a strong preference of the Fe atoms for the $8f$ sites. In an ideally stoichiometric and ordered compound the $8f$ sites are fully occupied by the Fe atoms, and the $8i$ and $8j$ sites by the Al atoms only. The rare-earth atom then sits at the center of a regular tetragonal prism surrounded by 8 Fe atoms (Fig. 1).

The first report on the magnetic properties of this family of compounds was given more than 20 years ago independently and almost simultaneously by Buschow and van der Kraan^{2,3} and by Felner and Nowik.⁴ The former reported bulk magnetization and Mössbauer measurements for a number of compounds and found that the Fe sublattice orders at temperatures between 135 and 200 K. The rare-earth atoms order at a much lower temperature, below 50 K. Due to the highly symmetrical environment of the $2a$ sites and the antiferromagnetic coupling of the Fe atoms, the molecular field acting on the rare-earth atoms is small. This would explain the lower ordering temperature of the rare earth compared to the transition-metal sublattice.

The ordering temperatures of LuFe_4Al_8 and YFe_4Al_8 were determined by Buschow and van der Kraan^{2,3} as 197.3 and 184.7 K, respectively, on the basis of Mössbauer data. However, the reported susceptibility curve of the Lu sample showed a well defined maximum at 100 K. Felner and Nowik, in turn, assigned an ordering temperature of 97 and 94 K to LuFe_4Al_8 and YFe_4Al_8 , respectively, deduced from magnetization measurements. The susceptibility curve of YFe_4Al_8 also showed an anomaly at 100 K. Although disagreeing in the Fe ordering temperature, both authors agreed that the ordering of the Fe atoms is antiferromagnetic, probably a modulated magnetic structure.⁴

A number of unusual magnetic phenomena have been observed and reported for the system $\text{YFe}_x\text{Al}_{12-x}$, namely an anomalous thermomagnetic behavior comparing the field-

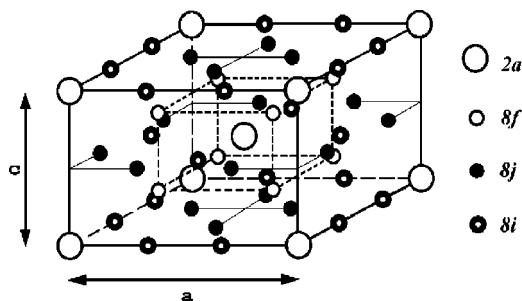


FIG. 1. Crystallographic unit cell of the ThMn_{12} -type structure. The f element occupies the $2a$ sites at the origin and body-centered positions. The other atoms occupy the $8f$, $8i$, and $8j$ sites.

cooled and zero-field-cooled curves, showing pronounced hysteretic behavior even in small applied fields.^{5–7} These have been attributed to partial disorder between the Fe and Al sites. Felner and Nowik,⁷ on the account of failure to observe any magnetic peaks on a powder neutron-diffraction experiment on YFe_5Al_7 proposed that the Fe disorder could produce a spin-glass state with no long-range order of the Fe moments. Powder neutron-scattering experiments on DyFe_4Al_8 (Ref. 8) and HoFe_4Al_8 (Refs. 9 and 10) were also interpreted in a spin-glass model. However, magnetic satellites were observed at low temperature and attributed to the Fe atoms. It should be born in mind that the samples used in these experiments had a disorder of Fe atoms into the $8i$ and $8j$ sites between 5 and 10%.

Since this early work, crystals of both rare-earth and uranium compounds with the ThMn_{12} type of structure became available.^{11–14} They have been used on more sophisticated neutron- and magnetic x-ray scattering experiments,^{15–18} which enabled much more detailed information to be obtained on the magnetic ordering and the nature of the interactions between the rare-earth and transition-metal sublattices, compared to older experiments on powders.

We have recently reported a single-crystal neutron study of DyFe_4Al_8 and HoFe_4Al_8 using both unpolarized and polarized neutrons.¹⁷ It was found that the Fe sublattice orders at 175 K with a moment of $1\mu_B$ in the ab plane in a cycloid magnetic structure with a propagation vector along $[110]$. At ~ 50 K (Dy) and 80 K (Ho) the rare-earth moment starts to order and follows the modulation of the Fe sublattice. At a lower temperature higher-order harmonics of the magnetic modulation develop due to a bunching of the cycloid modulation of the rare-earth atoms along high-symmetry directions. Although the magnetic ordering is long range, giving rise to sharp magnetic peaks, a non-negligible fraction of the rare-earth moment appears as diffuse scattering beneath the Bragg peaks. It was also found that the modulated magnetic structure of the rare-earth atoms is easily distorted under any small applied magnetic field, explaining the unusual sensitivity to small fields. The modulation on the Fe sublattice is much more stable and remains unperturbed in fields up to at least 5.5 T.

Pursuing these studies, we have been interested also in the isostructural compounds with a nonmagnetic heavy atom, such as are LuFe_4Al_8 and YFe_4Al_8 . Unfortunately, both the available Lu and Y crystals were of much worse quality than the U, Dy, and Ho ones, and found to be twinned. A brief account on preliminary neutron-scattering experiments performed has appeared.¹⁵ The Fe atoms order in a modulated magnetic structure, with a propagation vector τ of the form $(\tau, \tau, 0)$, $\tau \sim 0.22$, below a transition temperature of 100 K. The relatively poor quality of the crystals, and also the fact that T_N appeared to be at variance with reported ^{57}Fe Mössbauer measurements, did not appear to justify a further neutron-scattering study.

Recently, a powder-diffraction study of the magnetic ordering on $M\text{Fe}_4\text{Al}_8$ was reported by Papamantellos *et al.* for $M = \text{La}, \text{Ce}, \text{Y}, \text{and Lu}$,¹⁹ and for $M = \text{Tb}$.²⁰ The Lu and Y polycrystalline samples ordered at a temperature of about 190 K, in agreement with the Mössbauer results, but a much

higher value than found by us on the single crystals. In both the single-crystalline and polycrystalline samples the modulation of the Fe atoms propagate along the $[110]$ directions. However, the wave vectors found on the powder work $(0.135, 0.135, 0)$ and $(0.145, 0.145, 0)$ for the Lu and Y samples, respectively, are much shorter than those measured on the single crystals, albeit being closer to the values found in DyFe_4Al_8 and HoFe_4Al_8 . This puzzling situation concerning the different results obtained from the polycrystalline and single-crystal samples prompted us to perform a better characterization of the crystals by other techniques, and also perform more detailed neutron studies. The unpolarized neutron experiments were complemented with a zero-field neutron polarimetry experiment on the Lu crystal which, combined with new Mössbauer spectroscopy results and single-crystal magnetization measurements, gives new insights into the problem.

We have now clear evidence that single-crystalline samples of LuFe_4Al_8 and YFe_4Al_8 produced by the Czochralski method by pulling a seed from a stoichiometric melt of the metals grow systematically off stoichiometry. The crystals end slightly enriched in Fe which partially substitutes Al at the crystallographic $8j$ sites.²¹ Probably as a result of frustration between the competing $8f$ - $8f$ and $8f$ - $8j$ interactions, the type of magnetic ordering at the $8f$ sites changes drastically and a substantially lower Néel transition temperature is found.

II. SAMPLE PREPARATION

The crystals were grown at ITN, Sacavém. The pure metals in stoichiometric proportions were melt under high purity argon in a tri-arc furnace on a water cooled copper crucible. The starting materials were used in the form of ingots with purity higher than 99.9%. The bulk charges were turned over and remelted at least twice to ensure homogeneity. The crystals were grown in an induction furnace with a levitation cold crucible by the Czochralski method, pulling a tungsten tip from the melt at a rate of ~ 2 cm/h and a rotation rate of 15 rpm. The samples used for neutron experiments have a typical cylinder shape with approximate dimensions 8.0 mm high and 2.0 mm diameter.

III. SINGLE-CRYSTAL MAGNETIZATION MEASUREMENTS

The susceptibility and magnetization curves were measured with a superconducting quantum interference device magnetometer (Quantum Design MPMS) along the a and c axis of a small single crystal extracted from the two larger samples that were used for the neutron-scattering experiments. The thermomagnetic $M(T)$ curves were measured under a small applied magnetic field ($H = 100$ Oe) while cooling under field (FC), and also on heating after zero-field cooling (ZFC). The magnetization curves $M(H)$ were measured at a set of various temperatures in the range 5–200 K up to a maximum field of 5.5, and the full hysteresis cycle was measured at 5.0 K. The magnetization and susceptibility curves of the Lu and Y crystal are very similar.

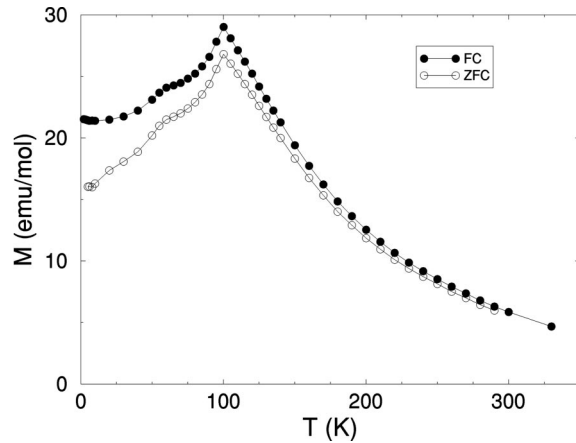


FIG. 2. $M(T)$ curves measured on a small single crystal of $\text{YFe}_{4.4}\text{Al}_{7.6}$ with an applied magnetic field of 100 Oe applied parallel to the c -axis cooling under field (full circles) and after zero field cooling (open circles).

Figure 2 shows the temperature dependence of the magnetization of the Y sample under a field of 100 Oe applied parallel to the c axis. A sharp anomaly is seen on the susceptibility curve at 100(2) K and another smaller anomaly occurs as a broader shoulder at 60(5) K. These two anomalies are seen on both the ZFC and FC curves and also when the field is applied along the a axis.

The magnetization curves are typical of an antiferromagnet, increasing almost linearly with field up to 5.5 T (Fig. 3). A comparison of the measurements performed along the a and c axis shows that the magnetic anisotropy is small. The full hysteresis cycle of the Y sample measured at 5 K is shown in the insert of Fig. 3. The hysteresis is very small and the remanence practically zero.

A fit of the inverse susceptibility in the paramagnetic range using a modified Curie-Weiss law, $\chi = \chi_0 + C/(T - \theta_p)$ gives an effective moment per iron atom of $4.30\mu_B$ and $\theta_p = -125$ K.

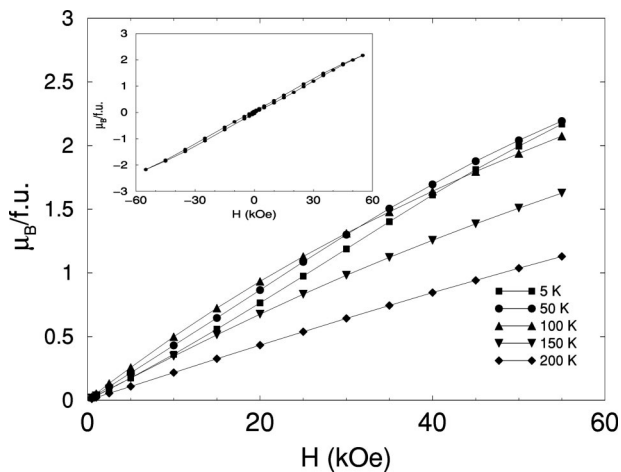


FIG. 3. $M(H)$ curve measured on a small single crystal of $\text{YFe}_{4.4}\text{Al}_{7.6}$ at temperatures 5, 50, 100, 150, and 200 K. The field was applied parallel to the c axis. The inset shows a full hysteresis cycle measured at 5 K.

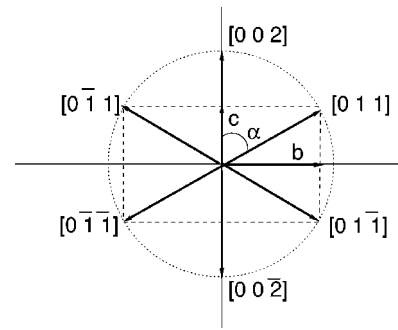


FIG. 4. Rotation of crystal axis underlying the twin law. The $[100]$ axis is perpendicular to the drawing plane. Notice α is close to 60° when $a \sim \sqrt{3}c$.

Magnetization and susceptibility measurements have been reported on a single-crystalline sample of YFe_4Al_8 also grown by Czochralski in another laboratory,¹¹ which showed a flat maximum of the susceptibility at 195 K and a rather pronounced increase of the susceptibility below 100 K. This was interpreted as weak ferromagnetism arising either from partial disorder of the Fe and Al atoms or as a canting of the antiferromagnetic moments at low temperatures.

IV. STRUCTURAL REFINEMENT

In order to better characterize the single crystals, particularly having in mind a precise determination of stoichiometry and amount of extinction, the intensities of a set of nuclear Bragg reflections were measured on the D15 diffractometer installed at Institut Laue-Langevin's High Flux Reactor. This two-axis diffractometer uses a wavelength of 1.172 \AA from a Cu(331) monochromator and works in normal-beam geometry, so that reflections out of the equatorial plane can be measured and much of reciprocal space is accessible. The samples were mounted on a standard aluminum sample holder and placed inside an ILL "orange cryostat" with the long axis of the crystal vertical and parallel to the ω axis of the diffractometer.

During the initial stages of the experiment it was found that both the Lu and Y crystals were twinned. An orientation matrix was obtained with the crystallographic $[0\bar{1}1]$ axis vertical but a number of reflections were found that could not be indexed as integer hkl by this matrix. However, these reflections could be indexed with another orientation matrix with the c axis vertical. No single orientation matrix could index all reflections, although a subset of them could be indexed with *either* of the two matrices. These reflections were broad and exhibited a split profile. It was concluded that the samples are twinned, each crystal consisting of a juxtaposition of two individual single-crystal grains, one having the $[0\bar{1}1]$ and the other the $[001]$ axis vertical.

The origin of the twinning can be found on the fact that the a and c cell parameters closely match the relation $a = \sqrt{3}c$. Thus the $[002]$ and $[0\bar{1}1]$ axis can easily be mismatched during crystal growth. Such a mismatch corresponds to a rotation of the crystal by circa 60° around the a axis as depicted in Fig. 4. This rotation is given in the crys-

tallographic direct space by the matrix

$$M = \begin{pmatrix} 1 & 0 & 0 \\ 0 & \frac{1}{2} & \frac{1}{2} \\ 0 & -\frac{3}{2} & \frac{1}{2} \end{pmatrix}. \quad (4.1)$$

The corresponding rotation in reciprocal space that transforms the hkl indices of a reflection of the grain with $[0\bar{1}1]$ vertical into those of a possibly overlapping reflection originating from the grain with the c axis vertical is $M' = \tilde{M}^{-1}$:

$$M' = \begin{pmatrix} 1 & 0 & 0 \\ 0 & \frac{1}{2} & \frac{3}{2} \\ 0 & -\frac{1}{2} & \frac{1}{2} \end{pmatrix}. \quad (4.2)$$

The above twin law was confirmed by performing rocking scans of several hkl reflections from one, the other, or both single-crystal grains. Figure 5 shows two such scans, one of a double reflection with contribution from both grains and another of a reflection originating from a single grain.

Having understood the twin law, an extensive set of nuclear intensities was measured to refine the crystal structure. A total of 850 and 574 reflections for the Lu and Y samples, respectively, were measured at a stabilized temperature of 2.0(5) K. The intensities were measured on wide ω scans, the reflection profiles integrated and corrected for the Lorentz factor using the ILL program COLL5N. No absorption corrections were performed due to the low absorption cross section of thermal neutrons of the two samples.

The least-squares refinement of the crystal structures was performed using the computer program SHELXL97.²² Each reflection was indexed as arising from one or the other of the two grains and for those points where the two reciprocal lattices coincide the program was instructed to calculate an intensity given by the sum of the contributions of the two individual grains, weighted by their volume fraction. The parameters that were refined in the structural model were the $8f$, $8i$, and $8j$ site occupancies, the x atomic coordinates of the $8i$ and $8j$ sites, the anisotropic Debye-Waller temperature factors, one extinction parameter and the relative volume fraction of the two grains. The total number of parameters refined was 20 but the data/parameter redundancy is comfortably large (>25). In the full-matrix least-squares refinement the minimized quantity was $\sum w(I_{\text{obs}} - I_{\text{calc}})^2$, $w = 1/[\sigma^2(I) + (pI)]^2$ where the instability factor p used to downweight the strongest reflections was adjusted to obtain a flat distribution of residuals with no bias towards the strongest reflections.

Once the twinning was taken into account, an excellent fit to the intensity data was obtained as shown by the low value of the residual indices measuring the discrepancy between the observed and calculated structure factors $R=2.72$ and

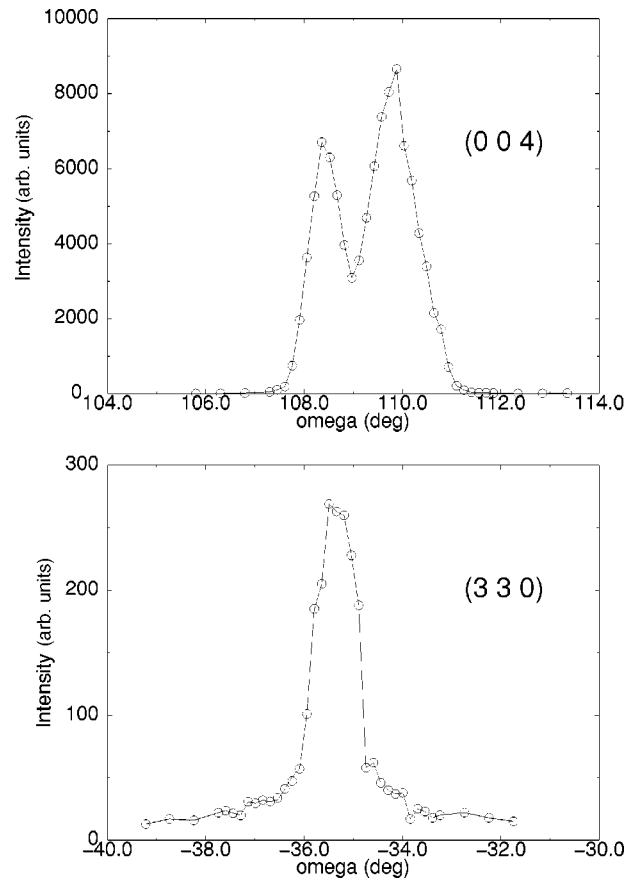


FIG. 5. Rocking scans through the 004 and 330 nuclear reflections of the twinned $\text{LuFe}_{4.4}\text{Al}_{7.6}$ crystal. The 330 reflection is a single peak, the 004 reflection shows a double peak structure, the second peak is the $0\bar{6}2$ reflection originating from the other twin crystal grain.

2.93 % for the Lu and Y samples, respectively. The results of the final cycle of the least-squares fits are given in Tables I and II. No significant correlations above 70% between the refined parameters were found on analysis of the inverted variance-covariance matrix. Extinction is small in both crystals, the intensity loss by extinction of the strongest reflection amounts to 19% but is negligible for most reflections.

Despite the twinning problem, the precision of the structural parameters of the single-crystal data is higher (except for cell parameters) compared to the powder data¹⁹ with estimated uncertainties four to five times smaller. However, the results match closely, except for the site occupancies. Indeed, there is clear evidence from the refinements that both single crystals of Lu and Y are off the ideal stoichiometry and that partial substitution of Fe by Al occurs at the $8j$ sites. As shown below, this is in agreement with the Mössbauer results and has an important effect on the magnetic properties. Within the accuracy of our data, the $8f$ sites and the $8i$ sites are fully occupied exclusively by Fe and Al atoms, respectively. The compositions obtained from the refined site occupancies are $\text{LuFe}_{4.38(4)}\text{Al}_{7.62(4)}$ and $\text{YFe}_{4.40(5)}\text{Al}_{7.60(5)}$. The relative volume fraction of the two individual grains forming the twinned crystals are in both samples close to

TABLE I. Crystallographic data for $\text{LuFe}_{4.4}\text{Al}_{7.6}$.

Atom	Site	x	y	z	Occ	B_{eq}
Lu	$2a$	0	0	0	1.0	0.24(4)
Fe	$8f$	1/4	1/4	1/4	1.02(1)	0.20(2)
Al	$8i$	0.3410(2)	0	0	0.99(1)	0.22(4)
Al	$8j$	0.2786(2)	1/2	0	0.906(8)	0.37(4)
Fe	$8j$				0.094(8)	

Space group: $I4/mmm$
 $a=b=8.644(3)$ Å $c=5.032(2)$ Å
 $R(F)=2.72\%$ $wR(F^2)=5.98\%$

80%:20%, the grain with the largest volume being that with c parallel to the growth axis of the crystal.

V. MÖSSBAUER SPECTROSCOPY

A small fragment taken out of the tip of the LuFe_4Al_8 single crystal used for neutron work was powdered. The resulting powder was pressed together with lucite powder into perspex holders, in order to obtain homogeneous and isotropic Mössbauer absorbers containing ~ 5 mg/cm² of natural iron. The ^{57}Fe Mössbauer-spectroscopy results were obtained in the transmission mode using a constant acceleration spectrometer and a 25 mCi ^{57}Co source in a Rh matrix. The velocity scale was calibrated using an α -Fe foil at room temperature. Spectra were collected at several temperatures between 300 and 5 K. Low-temperature spectra were obtained using a flow cryostat with temperature stability of ± 0.5 K. The spectra were fitted to Lorentzian lines using a modified version of the nonlinear least-squares method of Stone.²³ The fitting procedure was the same used in the case of the $\text{UFe}_x\text{Al}_{12-x}$ intermetallics and is described in detail elsewhere.²⁴

The Mössbauer spectra of this sample, taken at 5 and 298 K (Fig. 6) are similar to those obtained for $\text{UFe}_{4.2}\text{Al}_{7.8}$ (Ref. 24) and $\text{YFe}_{4.2}\text{Al}_{7.8}$.²¹ Particularly, the presence of at least two magnetic splittings is clear in the spectrum at 5 K. This feature, typical of $M\text{Fe}_x\text{Al}_{12-x}$ ($M=\text{U},\text{Y}, 4.2 \leq x \leq 4.4$) intermetallics, reveals the occupation of a small fraction of the $8j$ sites by the Fe atoms in agreement with the structural refinement based on the neutron data.

The Mössbauer spectra of these compounds (as well as those containing more Fe) have been successfully analyzed assuming that the magnetic hyperfine fields, B_{hf} of the Fe atoms depend not only on the crystallographic site but also on the number of the Fe nearest neighbors (NN). The probabilities of the configurations, corresponding to different numbers of Fe NN, have been calculated for the $M\text{Fe}_x\text{Al}_{12-x}$ ($M=\text{U},\text{Y}, 4.2 \leq x \leq 4.4$) intermetallics assuming full occupancy of the $8f$ sites by Fe and random occupation of the $8j$ sites by Al and the remaining Fe atoms.²⁴

Using the same model, several fits to the spectra of the Lu sample were performed assuming compositions $\text{LuFe}_x\text{Al}_{12-x}$ ($x=4.1, 4.2, 4.3,$ and 4.4). A significantly better fit was obtained for the composition $\text{LuFe}_{4.3}\text{Al}_{7.7}$. The estimated hyperfine parameters are summarized in Table III. The increase of the estimated isomer shifts δ with increasing number of Fe NN are similar to those observed for the Y and U analogs. These trends may be understood on the basis of the Fe-Fe intersite exchange interactions and of the decrease of the electron density at the Fe nuclei, respectively.²⁴

The spectra obtained between 60 and 90 K (Fig. 6) could only be fitted by a continuous distribution of B_{hf} . Either a true continuous distribution of hyperfine fields is present or a large number of different B_{hf} which cannot be resolved. Assuming that μ_{Fe} are proportional to B_{hf} this suggests that, in this temperature range, there is either an incommensurate distribution of μ_{Fe} values or, at least, a large number of different values. Below 60 K the distribution of hyperfine fields sharpens and at 5 K the spectra could be reasonably fit

TABLE II. Crystallographic data for $\text{YFe}_{4.4}\text{Al}_{7.6}$.

Atom	Site	x	y	z	Occ	B_{eq}
Y	$2a$	0	0	0	1.0	0.35(6)
Fe	$8f$	1/4	1/4	1/4	1.02(2)	0.26(2)
Al	$8i$	0.3410(3)	0	0	1.00(2)	0.27(6)
Al	$8j$	0.2787(2)	1/2	0	1.00(1)	0.44(6)
Fe	$8j$				0.094(8)	

Space group: $I4/mmm$
 $a=b=8.669(9)$ Å $c=5.030(9)$ Å
 $R(F)=2.93\%$ $wR(F^2)=5.86\%$

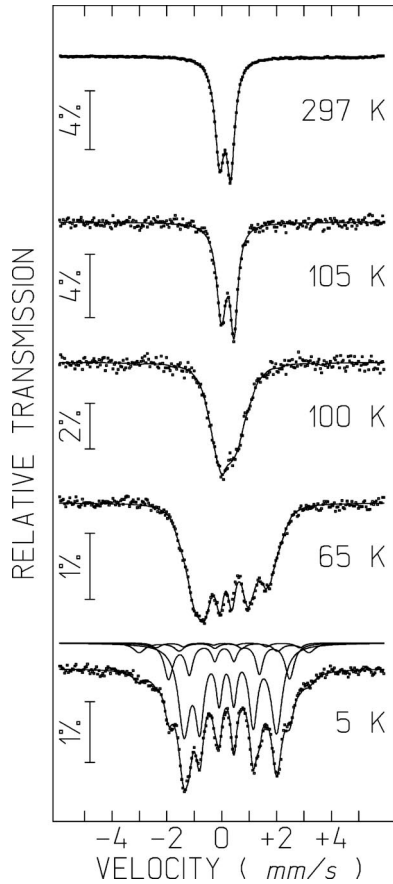


FIG. 6. Mössbauer spectra from powder of a fragment of the $\text{LuFe}_{4.4}\text{Al}_{7.6}$ single crystal, as function of temperature.

with only three different μ_{Fe} values for the YFe_4Al_8 sample and four values for the LuFe_4Al_8 one.

VI. UNPOLARIZED-NEUTRON EXPERIMENTS

A survey of reciprocal space searching for magnetic reflections at low temperature was performed on the D15 dif-

TABLE III. Estimated parameters from the Mössbauer spectrum of the $\text{LuFe}_{4.3}\text{Al}_{7.7}$ sample taken at 5 K. The relative areas I are fixed at consistent values with the calculated probabilities for the different number of Fe nearest neighbors (NN) on the $8f$ and $8j$ sites. The isomer shift δ is relative to metallic $\alpha\text{-Fe}$ at 295 K; $\epsilon = (e^2V_{zz}Q/4)(3\cos^2\theta - 1)$ is the quadrupole shift calculated from $(\phi_1 + \phi_6 - \phi_2 - \phi_5)/2$ where ϕ_n is the shift on the n th line of the magnetic sextet due to quadrupole coupling. Γ is the linewidths of the two inner peaks of a sextet and B_{hf} the magnetic hyperfine field. Estimated errors for the sextets with $I > 11\%$ are ≤ 0.2 T for B_{hf} , ≤ 0.02 mm/s for δ , ϵ , Γ and for the others ≤ 0.4 T for B_{hf} , ≤ 0.03 mm/s for δ , and ≤ 0.04 mm/s for Γ and ϵ .

Site	NN	I (%)	δ (mm/s)	ϵ (mm/s)	Γ (mm/s)	B_{hf} (T)
$8j$	≥ 4	7.9	0.21	-0.15	0.33	19.3
$8f$	≥ 3	2.8	0.22	-0.11	0.30	16.3
$8f$	≥ 3	21.8	0.23	-0.17	0.30	13.8
$8f$	2	67.5	0.29	-0.14	0.28	10.5

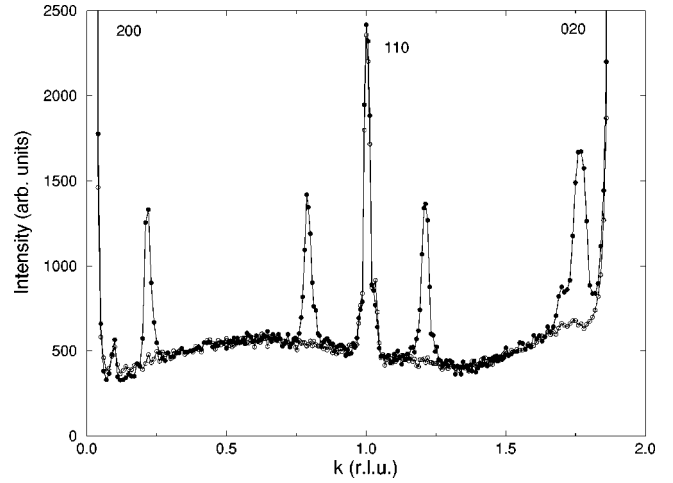


FIG. 7. Scans along the $h\bar{h}0$ direction from 020 to 200 measured in the $\text{LuFe}_{4.4}\text{Al}_{7.6}$ sample at 3.0 K (solid points) and 150 K (open points). The strong 200 and 020 nuclear reflections have a peak intensity of $\sim 200\,000$ and are truncated on the expanded scale.

fractometer, using a wavelength of 1.172 Å. Several reciprocal-lattice scans were made along the main symmetry directions of the Brillouin zone centered around a few reciprocal lattice points with small hkl indices. The reciprocal-lattice scans along the line $200 \rightarrow 020$ for the Lu and Y crystals are shown in Figs. 7 and 8, respectively.

Symmetric pairs of satellites occur around the nuclear peaks corresponding to a propagation vector of the form $\tau = (\tau, \tau, 0)$, similarly to what was found in DyFe_4Al_8 ,¹⁷ HoFe_4Al_8 ,¹⁷ TbFe_4Al_8 ,²⁰ and on stoichiometric LuFe_4Al_8 and YFe_4Al_8 polycrystalline samples.¹⁹ The τ value is 0.212(5) and 0.226(5) r.l.u. for the Lu and Y crystals and is practically independent of temperature within the Q resolution of our experiments. These values are much larger than

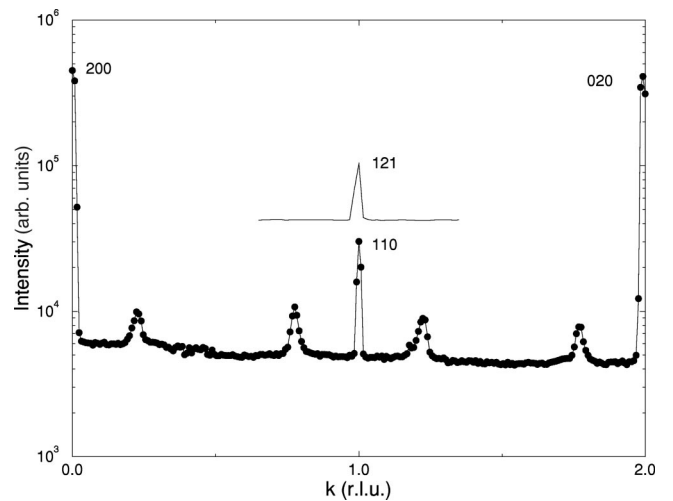


FIG. 8. Scan along the $h\bar{h}0$ direction from 020 to 200 measured in the $\text{YFe}_{4.4}\text{Al}_{7.6}$ sample. Note that the intensity is plot on a logarithmic scale. A similar reciprocal-lattice scan passing through the 121 reflection and showing the absence of satellites is presented for clarity on an offset scale.

those found previously in these types of compounds, for which $\tau \sim 0.133\text{--}0.145$.

No satellites are observed around reciprocal-lattice points with $h+k+l$ odd. This means that the magnetic structure fulfills the body centering rule, and therefore the Fe atoms which are related by the body centering operators must have a phase shift that is simply given by $2\pi\tau \cdot (\frac{1}{2}, \frac{1}{2}, \frac{1}{2}) = 2\tau\pi$.

The magnetic ordering lowers the symmetry of the system, as the propagation vector does not remain invariant under the tetragonal fourfold rotation. Therefore the 8 Fe atoms in the unit cell are split into two nonequivalent sets:

$$\begin{array}{cccc} & 1 & 2 & 3 & 4 \\ \text{Fe1 at} & \frac{1}{4}, \frac{1}{4}, \frac{1}{4} & \frac{1}{4}, \frac{1}{4}, \frac{3}{4} & \frac{3}{4}, \frac{3}{4}, \frac{1}{4} & \frac{3}{4}, \frac{3}{4}, \frac{3}{4} \\ \text{Fe2 at} & \frac{1}{4}, \frac{3}{4}, \frac{1}{4} & \frac{1}{4}, \frac{3}{4}, \frac{3}{4} & \frac{3}{4}, \frac{1}{4}, \frac{1}{4} & \frac{3}{4}, \frac{1}{4}, \frac{3}{4} \end{array} \quad (6.1)$$

The moments of these two sublattices are not *symmetry* constrained to have equal values or be parallel and there will be, in general, a phase shift ϕ between the modulations of the Fe1 and Fe2 sublattices.

If the phase difference between the Fe1 and Fe2 representative atoms at $\frac{1}{4}, \frac{1}{4}, \frac{1}{4}$ and $\frac{1}{4}, \frac{3}{4}, \frac{1}{4}$ corresponds to $2\pi\tau \cdot (\mathbf{r}_{\text{Fe2}} - \mathbf{r}_{\text{Fe1}}) = \tau\pi$ then the structure factor for those reflections with h or k odd will be zero and magnetic satellites would occur only around nuclear Bragg reflections with h and k even—the so-called *F* mode.

In the cases of DyFe_4Al_8 and HoFe_4Al_8 we have found that the magnetic satellites only exist around those hkl reflections with h and k odd arising from the Fe moments. This indicates that the modulation of the Fe2 sublattice has an extra π phase shift with respect to that of Fe1, i.e., $\Phi = \tau\pi + \pi$, corresponding to the so-called *G* antiferromagnetic mode.

For the two off-stoichiometric crystals of Lu and Y now under study, the satellites are found around *both* types of reflections, as shown in Figs. 7 and 8, which means that the phase shift between the Fe1 and Fe2 atoms is not one of the special cases where $\phi = \tau\pi$ or $\phi = \tau\pi + \pi$. However, the satellites are *not* seen around hkl indices with mixed h and k parities, which shows that the moments on the sites 1 and 2 and 3 and 4 are parallel.

The temperature dependence of the intensity of the $1\bar{1}0^+$ satellites for the Lu and Y samples are shown in Figs. 9 and 10. The magnetic intensity is not yet saturated at the lowest temperature attained in the experiment (1.9 K) but it was found to decrease on warming rather smoothly and vanishes at 100(3) K. This value for the Néel temperature is in good agreement with that obtained from the susceptibility measurements and Mössbauer data. The second magnetic anomaly at 60 K of the susceptibility curves, also noticed on the Mössbauer measurements, does not show clearly on the I vs T curves.

We have searched for any other components of the magnetic modulation, particularly for higher-order harmonics, but none were found. As can be seen in Fig. 7 the intensity of the weak 110 reflection is virtually the same at 2.0 and 150 K

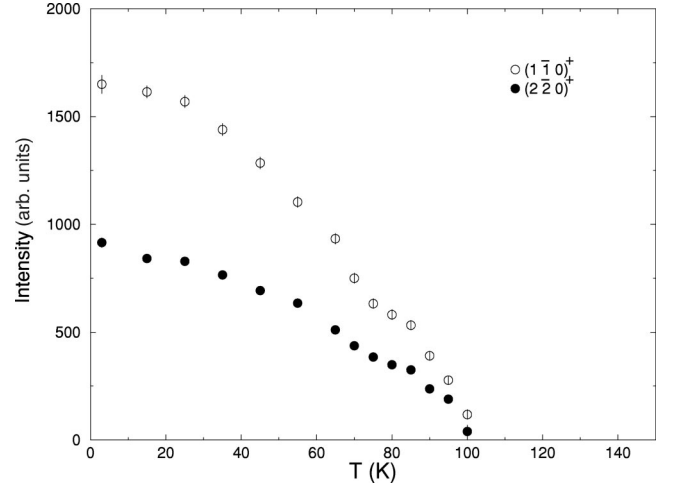


FIG. 9. Temperature dependence of the $1\bar{1}0^+$ and $2\bar{2}0^+$ magnetic satellites of $\text{LuFe}_{4.4}\text{Al}_{7.6}$.

for the Lu crystal. This excludes the possibility of a second antiferromagnetic $\tau=0$ component that has been reported in stoichiometric LuFe_4Al_8 but not in YFe_4Al_8 .¹⁹

VII. NEUTRON ZERO-FIELD POLARIMETRY

The single crystal of LuFe_4Al_8 was examined on the three-dimensional zero-field polarimeter CRYOPAD-II installed on the sample table of the neutron triple-axis spectrometer IN20 at the ILL.

We have recently discussed in detail the application of zero-field polarimetry to study the noncollinear magnetic structure of DyFe_4Al_8 which unambiguously established the form of the magnetic modulation as a cycloid propagating along $[110]$ with the moments rotating in the (001) plane. A thorough description of CRYOPAD and zero-field neutron polarimetry is available.²⁵ Here we shall only give a brief discussion and show the results obtained on a similar experiment performed on the LuFe_4Al_8 sample.

The polarization of scattered neutrons depends on the

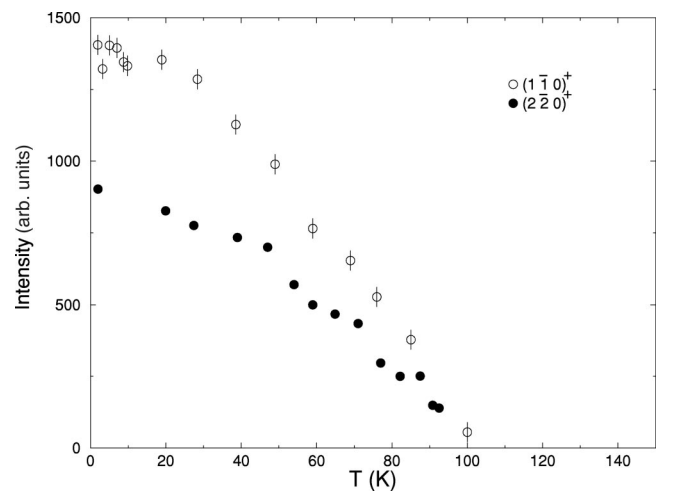


FIG. 10. Temperature dependence of the $1\bar{1}0^+$ and $2\bar{2}0^+$ magnetic satellites of $\text{YFe}_{4.4}\text{Al}_{7.6}$.

relative orientation of the magnetic interaction vector \mathbf{Q} with respect to the polarization of incident neutrons.²⁶ The magnetic interaction vector is defined as

$$\mathbf{Q} = \hat{\boldsymbol{\kappa}} \times \left(\int \mathbf{M}(\mathbf{r}) \exp(i\boldsymbol{\kappa} \cdot \mathbf{r}) d^3\mathbf{r} \right) \times \hat{\boldsymbol{\kappa}}, \quad (7.1)$$

where $\mathbf{M}(\mathbf{r})$ is the magnetization distribution and $\hat{\boldsymbol{\kappa}}$ is a unit vector in the direction of the scattering vector. In general, \mathbf{Q} is a complex vector, $\mathbf{Q} = \mathbf{A} + i\mathbf{B}$. For a *collinear* structure \mathbf{A} is parallel to \mathbf{B} , but for a helix or a cycloid \mathbf{A} and \mathbf{B} are perpendicular.

For an amplitude modulated wave the polarization \mathbf{P}_f scattered by a pure magnetic reflection with $\mathbf{Q} \parallel \mathbf{Q}^*$ is related to the incident polarization \mathbf{P}_i by precession through π around the magnetic interaction vector \mathbf{Q} . When \mathbf{Q} and \mathbf{Q}^* are not parallel, such as in an helix or cycloid structure, the situation is different. In this case, if \mathbf{P}_i is perpendicular to $\boldsymbol{\kappa}$ then the polarization is flipped around the longer component of \mathbf{Q} and rotated towards the scattering vector by an angle which depends on the quantity $2\boldsymbol{\kappa} \cdot (\mathbf{A} \times \mathbf{B}) / (A^2 + B^2)$.

In general the sample contains several magnetic domains, and the scattered polarization is an average of the output polarization scattered by each domain weighted by its volume fraction.

Because of our previous experience,¹⁷ the crystal was mounted with the $[1\bar{1}0]$ axis vertical and $[110]$ and $[001]$ in the scattering plane in a variable temperature cryostat inside the zero-field region of the polarimeter. The magnitude and direction of the polarization scattered by seven Bragg reflections of the form $h \pm \tau, h \pm \tau, l$ were determined at 4.0 K with the incident polarization parallel to each of the *polarization* axis in turn. The polarization axes are defined with z vertical, x parallel to the scattering vector and y at right angles completing a right-handed Cartesian set.

The largest count rate at the detector of a magnetic satellite was only 2 cps and in order to obtain sufficient statistics the measurements of each reflection lasted for several hours.

The results are shown in Table IV and the major features can be summarized as follows:

- (i) There is no significant rotation of the polarization.
- (ii) There is no significant depolarization of the scattered beam when the incident polarization is parallel to the scattering vector (x axis).
- (iii) For all reflections, the polarization of the scattered beam is reversed when the incident polarization is parallel to x or z , but not when it is parallel to y .
- (iv) The scattered beam is depolarized to some extent when the incident polarization is parallel to y or z . The depolarization is greatest for those reflections with $l=0$.

From these results one can deduce the following characteristics of the magnetic structure. From (i) and the fact that depolarization is observed, it can be deduced that antiferromagnetic domains are present, and equally occupied. Observation (ii) should always be true for pure antiferromagnetic reflections. Observation (iii) indicates that the largest component of the moments lie in the (110) plane containing the propagation vector and the c axis. Observation (iv) shows that there must be a component of the moment parallel to the

c axis. To give the observed result, the major component of the moment must lie along $[110]$. There must also be a component parallel to c and a smaller one in the $[1\bar{1}0]$ direction perpendicular to the scattering vector.

Overall, these observations are *incompatible* with a cycloidal model where the Fe moments rotate in the (001) planes as found in DyFe_4Al_8 , HoFe_4Al_8 , TbFe_4Al_8 , and in stoichiometric YFe_4Al_8 . In such a case the polarization of the $hh0$ reflections is reversed when incident parallel to x and y and remains unchanged when incident parallel to z . Furthermore, and for a cycloid with low ellipticity and an equipartition of domain population, a large depolarization of the beam would be expected for the 112^+ satellites, because for this reflection the real and imaginary components of the magnetic interaction vector would have a comparable magnitude. Both these effects have been observed in measurements performed on DyFe_4Al_8 above the ordering temperature of the rare earth, where the Fe modulation is indeed a cycloid with the moments rotating in the tetragonal basal plane. One would expect the same situation to occur for the double-cone cycloidal model proposed for stoichiometric LuFe_4Al_8 ,¹⁹ where an alternating $+ - + -$ G -type antiferromagnetic component parallel to c is added to the rotation of the moments in the basal plane. The extra $\tau=0$ component observed in stoichiometric LuFe_4Al_8 , if present in our sample, would not change the picture here, because this component does not interfere with the polarimetric measurements of the satellites, in the same way as it does not interfere with the intensities of these magnetic reflections.

A smaller subset of polarimetric data was also measured at 70 K. The results are similar, within statistics, to those measured at low temperature.

VIII. MAGNETIC STRUCTURE REFINEMENT

A cycloidal magnetic structure with the moments rotating in the (001) plane, such as found in DyFe_4Al_8 , HoFe_4Al_8 , and YFe_4Al_8 is in disagreement with the polarimetric measurements on the Lu crystal. The simplest model for the magnetic structure that could explain the observed reversal of the polarization around the z axis is a cycloid with the moments rotating in the diagonal (110) plane containing the propagation vector and the c axis. However, this model cannot explain the observed depolarization of the beam, particularly for the $l=0$ reflections. This requires that the major components of the moments lie in the (110) plane containing the propagation vector. There must exist a component along c and a smaller component along $(1\bar{1}0)$. All together, these requirements can only be fulfilled by a magnetic structure with a rather low symmetry, which rules out any cycloidal model where the moments are constrained along a symmetry plane of the unit cell. A lower symmetry modulated magnetic structure is that of an amplitude modulated wave, which we find more likely in this case.

We have refined a possible model for the magnetic structure satisfying the above-mentioned requirements, starting from an amplitude modulated wave with the moments in the (110) plane but allowing for a tilt out of this plane. As a first approximation, the moments of all Fe atoms were con-

TABLE IV. CRYOPADII polarimetric data for $\text{LuFe}_{4.38}\text{Al}_{7.62}$. P_i and P_f are the polarization vectors of the incident and scattered beams. The polarization axes are $x\parallel\boldsymbol{\kappa}$, y is in the scattering plane containing $[110]$ and $[001]$, perpendicular to $\boldsymbol{\kappa}$ and z is vertical and parallel to $[1\bar{1}0]$. P_c is the scattered polarization calculated from the magnetic structure model of an amplitude modulated wave discussed in the text. The estimated error bars on the incident and scattered polarizations are ± 0.02 and ± 0.06 , respectively.

h	k	l	P_i			P_f			P_c		
			x	y	z	x	y	z	x	y	z
-1.22	-1.22	0.00	0.00	0.00	0.90	0.18	0.07	-0.64	0.00	0.00	-0.54
			0.90	0.00	0.00	-0.85	0.02	0.14	-0.90	0.00	0.00
			0.00	0.90	0.00	0.35	0.75	0.03	0.00	0.54	0.00
-1.78	-1.78	0.00	0.00	0.00	0.90	0.03	0.13	-0.50	0.00	0.00	-0.54
			0.90	0.00	0.00	-0.93	-0.20	-0.05	-0.90	0.00	0.00
			0.00	0.90	0.00	0.08	0.56	0.01	0.00	0.55	0.00
-1.22	-1.22	2.00	0.00	0.00	0.90	0.06	0.03	-0.86	0.00	0.08	-0.90
			0.90	0.00	0.00	-0.73	-0.32	0.02	-0.90	0.00	0.00
			0.00	0.90	0.00	0.03	0.79	-0.07	0.00	0.90	0.08
-1.78	-1.78	2.00	0.00	0.00	0.90	0.04	-0.01	-0.81	0.00	0.09	-0.89
			0.90	0.00	0.00	-0.90	-0.16	0.02	-0.90	0.00	0.00
			0.00	0.90	0.00	-0.12	0.74	0.08	0.00	0.90	0.09
-0.78	-0.78	2.00	0.00	0.00	0.90	-0.04	0.01	-0.87	0.00	0.08	-0.90
			0.90	0.00	0.00	-0.91	0.30	-0.12	-0.90	0.00	0.00
			0.00	0.90	0.00	-0.19	0.81	0.03	0.00	0.90	0.08
-2.22	-2.22	2.00	0.00	0.00	0.90	0.04	0.01	-0.72	0.00	0.10	-0.89
			0.90	0.00	0.00	-0.91	-0.07	-0.10	-0.90	0.00	0.00
			0.00	0.90	0.00	0.20	0.69	0.08	0.00	0.90	0.10
0.22	0.22	2.00	0.00	0.00	0.90	0.04	0.00	-0.85	0.00	0.08	-0.90
			0.90	0.00	0.00	-0.93	0.00	-0.02	-0.90	0.00	0.00
			0.00	0.90	0.00	-0.01	0.90	0.01	0.00	0.90	0.08
-1.22	-1.22	-2.00	0.00	0.00	0.90	0.03	0.01	-0.83	0.00	-0.08	-0.90
			0.90	0.00	0.00	-0.85	0.15	-0.01	-0.90	0.00	0.00
			0.00	0.90	0.00	0.04	0.67	-0.09	0.00	0.90	-0.08
-0.78	-0.78	-2.00	0.00	0.00	0.90	0.07	-0.13	-0.88	0.00	-0.08	-0.90
			0.90	0.00	0.00	-0.99	0.16	0.10	-0.90	0.00	0.00
			0.00	0.90	0.00	-0.07	0.88	-0.03	0.00	0.90	-0.08

strained to be parallel and the amplitudes of the modulations of the two independent Fe magnetic sublattices to be equal, although as shown in Sec. V this is not an absolute requirement of symmetry. A least-squares fit of this model to the polarimetric observations was performed using the least-squares program PALSQ which is based on the CCSL library.²⁷ A reasonable agreement, with a $\chi^2=8.2$, between the calculated and observed final polarizations (respectively, P_c and P_f in Table IV) was obtained for the following set of polar angles describing the direction of the moments $\theta=94.7(1)^\circ$ and $\phi=47.3(5)^\circ$ (Table IV). This corresponds to a small tilt of $4.7(1)^\circ$ of the moments towards the c axis

and a $2.3(5)^\circ$ rotation out of the (110) plane. If we allow the two Fe moments to be nonparallel, the tilt angle of the Fe1 is practically unchanged and that of Fe2 atom becomes close to 10° but the introduction of the two extra angular parameters is not justified by a significant decrease of the χ^2 of the fit.

Although zero-field polarimetry is very sensitive to the directions of the magnetic moments it cannot give absolute values for the magnetic moments. Therefore the small set of integrated intensities of the magnetic satellites of the Lu crystal was put on an absolute scale by comparison with the nuclear reflections, and combined with the information derived from the polarimetry results to obtain the amplitude of

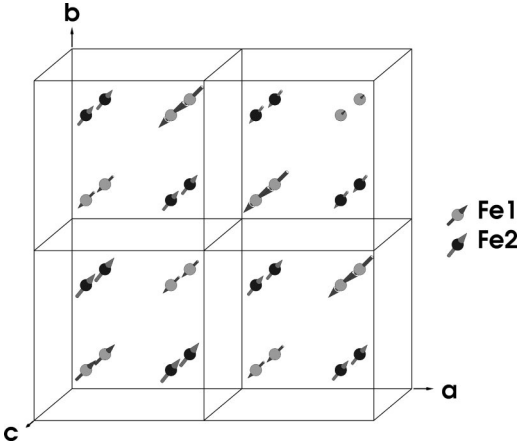


FIG. 11. Magnetic structure of $\text{LuFe}_{4.4}\text{Al}_{7.6}$ as deduced from a combined refinement of polarimetric and magnetic intensity data. The Fe moments are close to the 110 direction but have a tilt angle of 2.3° out of this direction in the (001) plane and an additional tilt of 4.7° out of this plane towards the c axis. See Eq. (6.1) for identification of Fe1 and Fe2.

the modulation of the Fe moments. Having fixed the directions of the moments to the values given by the polarimetric measurements, the moment of the Fe atoms and the phase shift between the Fe1 and Fe2 modulations were refined by least squares using the program MAGLSQ. The refined value for the Fe moment was $1.3(1)\mu_B$ and the phase difference between the Fe1 and Fe2 atoms is $25(10)^\circ$. The final residual factor between the observed and calculated intensities is relatively large ($R=21\%$), but the intensity data was sparse and of rather low quality. A drawing of the magnetic structure of the amplitude modulated wave that best fits both CRYOPAD and the intensity data is shown in Fig. 11. We have also considered the alternate cycloidal model with the moments rotating in the (110) plane, which gave a worse fit to the intensity data, $R=31\%$.

IX. DISCUSSION

We report a study of the magnetic properties of $\text{LuFe}_{4.4}\text{Al}_{7.6}$ and $\text{YFe}_{4.4}\text{Al}_{7.6}$, by means of magnetization measurements, Mössbauer spectroscopy, and both unpolarized and polarized single-crystal neutron-scattering experiments. The samples, which were grown by the Czochralski method starting from bulk charges with nominal 1:4:8 compositions, were intended to be single crystals of the nominal composition, but ended slightly enriched in Fe. We have shown that the small excess of Fe has a pronounced effect on the magnetic properties of these compounds.

Using single-crystal neutron diffraction, we have shown that the excess of Fe atoms substitutes Al atoms only at positions $8j$. The consequences of such a small substitution, that does not exceed 5% of the Al atoms, are a strong reduction of the Néel temperature from 190 to 100 K. This stoichiometry is consistent with the interpretation of the Mössbauer spectra.

Retrospectively, it appears very likely that many of the disparate results spread in the literature since the first reports

on these compounds concerning, e.g., the value of the Néel temperature of YFe_4Al_8 and LuFe_4Al_8 , may be due to a similar problem. Depending on the annealing conditions, even polycrystalline samples prepared from stoichiometric bulk charges tend to deviate from the ideal composition, probably due to the fact that stoichiometric YFe_4Al_8 and LuFe_4Al_8 do not melt congruently. For instance, we have found that only after annealing a stoichiometric bulk charge for a long time at a relatively high temperature (~ 1000 K) we could obtain a single-phase polycrystalline and stoichiometric sample.²¹

Similarly to the stoichiometric compounds, the Fe atoms order in a modulated magnetic structure with a wave vector τ of the form $(\tau\tau 0)$. The value of $\tau \sim 0.22$ is, however, about twice that found in the stoichiometric compounds. Since these values of τ presumably represent nesting wave vectors of the Fermi surface topology, it is not surprising that addition of Fe changes the shape of Fermi surface. Moreover, the propagation vectors in the Lu and Y compounds are found to be $\tau = 0.212(5)$ and $0.226(5)$, respectively, and both crystals are off-stoichiometric $M\text{Fe}_{4+\delta}\text{Al}_{8-\delta}$ by $\delta = 0.40$. Another important consequence of $\delta > 0$ is that the phase angle between the two Fe sublattices changes from π to $\sim 25^\circ$. Presumably this is related to the complex exchange paths set up by the additional Fe on the $8j$ site.

Using unpolarized neutron scattering ($\text{LuFe}_{4.4}\text{Al}_{7.6}$ and $\text{YFe}_{4.4}\text{Al}_{7.6}$) and zero-field neutron polarimetry ($\text{LuFe}_{4.4}\text{Al}_{7.6}$), we have shown that the *direction* of the Fe moments is also different from the stoichiometric compounds. According to a recent neutron powder-diffraction study,¹⁹ YFe_4Al_8 has a magnetic structure that is a cycloid with the moments rotating in the (001) plane and that of LuFe_4Al_8 has superimposed an extra $\tau = 0$ G -type antiferromagnetic component resulting on a double-cone cycloid structure. Neither of these structures can apply to the off-stoichiometric $\text{LuFe}_{4.4}\text{Al}_{7.6}$ because they are not compatible with the results of the zero-field neutron polarimetry study.

Although we cannot rule out other magnetic structures that could explain as well the polarimetric results, it appears that the most likely magnetic structure is that of an amplitude modulated wave with the Fe moments almost parallel to the [110] direction but with a small tilt of this axis in the (001) plane and also a small component towards the c axis.

The Mössbauer experiments of $\text{LuFe}_{4.4}\text{Al}_{7.6}$ have demonstrated that on cooling below ~ 60 K there is a distinct sharpening of the spectra; this has the consequence that the distribution of magnetic moments required for the fit is reduced to a small number of single B_{hf} values. At the lowest temperatures only four different magnitudes of the Fe hyperfine field, ranging from 10.5 to 19.3 T are required to simulate the experimental data (see Table III and Fig. 6). Such an interpretation is at variance with the model proposed from the analysis of the neutron data. This interpretation proposes an amplitude-modulated wave. Since the modulation wave vector is incommensurate, such an amplitude modulated structure would result in *all* possible magnitudes of the Fe moments. In examining this apparent contradiction between

the two measurements we have to be aware of the experimental limitations. From the physics aspect, we would expect some change of the modulation on lowering the temperature as the energy cost in entropy at the lowest temperature to maintain nonuniform magnetic moments is considerable. Normally, one or both of two effects are observed. First, the modulation becomes commensurate. This is outside our statistics, as the likely values would be 0.20 or 0.25, rather than the observed 0.212(5). Second, the modulation would tend to “square” as the temperature is lowered. Such a squaring results in high-order Fourier components, which would be seen, in particular, as a contribution at 3τ . For a perfect square-wave modulation the amplitude ratio A_3/A_1 between the first- and third-order harmonics is $\sim 1/3$, so that the intensity of the third-order satellite is roughly 10% of that of the first. Looking at Fig. 7, we would then expect to observe peaks of ~ 80 cts on the scale of the figure at the positions of the third-order satellites. They are not observed on this scale. However, this is for a complete square wave; a partial squaring, which would still be consistent with the Mössbauer results, might result in a peak of only 50% of this, i.e., 40 cts on a background of 500. Clearly, we are now entering the statistics of these neutron-scattering experiments on D15. Furthermore, the third-order peaks are frequently broader in momentum space than the first-order, further reducing their signal/noise ratio. When these various effects are considered, in addition to the twinning of the crystals, the apparent contradiction between the neutron and Mössbauer results should be treated with caution. Better crystals, together with a diffractometer such as D10, which has a lower background than D15,¹⁷ would be needed to test these ideas further. Of course, the analysis of the data from the neutron polarimeter derives *only* from the first-order satellites, so, by definition, only one Fourier component is considered. A further discussion of this can be found in Ref. 17.

Finally, we note that both in Figs. 9 and 10, which shows the temperature dependencies of the first-order satellites, there are some apparent unusual intensity variations, between 60 and 70 K in $\text{LuFe}_{4.4}\text{Al}_{7.6}$, and at a somewhat lower temperature in the Y compound. Given the statistics of these measurements, we cannot extract further information, but they may well indicate changes in the form of the magnetic modulation, again consistent with the Mössbauer results.

The off-stoichiometric Lu and Y samples have rather similar magnetic behavior, which is not totally unexpected if one considers that they are very close in composition. Moreover, the two heavy elements are both nonmagnetic, closely match in atomic radius and contribute the same number of electrons to the conduction band. Although we have not performed a study of the $\text{YFe}_{4.4}\text{Al}_{7.6}$ crystal at the level of detail as that of $\text{LuFe}_{4.4}\text{Al}_{7.6}$, it appears that the major difference in the magnetic structure concerns a small difference of the

magnitude of the propagation vector of the modulation.

The value of the ordered Fe moment is close to that found in other related compounds such as DyFe_4Al_8 ,¹⁷ HoFe_4Al_8 ,¹⁷ UFe_4Al_8 ,¹⁶ UFe_5Al_7 ,²⁸ and $\text{UFe}_{10}\text{Si}_2$,²⁹ but is lower than the value of $2.0\mu_B$ found in the neutron powder diffraction of stoichiometric LuFe_4Al_8 and YFe_4Al_8 ,¹⁹ which is closer to the full Fe moment. It is noteworthy that in DyFe_4Al_8 ,^{3,17} HoFe_4Al_8 ,^{3,17} $\text{UFe}_{10}\text{Si}_2$,²⁹ $\text{YFe}_{4.4}\text{Al}_{7.6}$, $\text{LuFe}_{4.4}\text{Al}_{7.6}$ (present study), where both single-crystal neutron diffraction and ⁵⁷Fe Mössbauer spectroscopy have been performed, the hyperfine coupling constant is close to $B_{hf}/\mu_{\text{Fe}} = 11 \pm 2 \text{ T}/\mu_B$. Considering that the B_{hf} are very similar ($\sim 11 \text{ T}$) in all the $M\text{Fe}_4\text{Al}_8$ compounds, and although B_{hf}/μ_{Fe} is not expected to be the same for all Fe-containing compounds,²⁹ it is still surprising that the μ_{Fe} in YFe_4Al_8 and in LuFe_4Al_8 estimated from powder diffraction are significantly larger than the $\mu_{\text{Fe}} \sim 1\mu_B$ estimated for the above referred ThMn_{12} intermetallics. It is well known that whereas the $8f$ - $8f$ site interaction is antiferromagnetic the presence of Fe at $8j$ sites favors a ferromagnetic alignment. Indeed, YFe_5Al_7 exhibits ferromagnetic behavior with a saturation magnetization of $\sim 1.3\mu_{\text{B}/\text{Fe}}$. A tendency towards ferromagnetism with increasing Fe concentration is also found in the $\text{UFe}_x\text{Al}_{12-x}$, $x > 4$ system. For a small excess of Fe, such as in our samples, a competition between an antiferromagnetic $8f$ - $8f$ coupling and a ferromagnetic $8f$ - $8j$ interaction might explain the observed decrease of T_N compared to the stoichiometric composition.

Despite the increased degree of complexity of both magnetic and crystallographic structures that can be handled nowadays by careful work on good resolution neutron powder-diffraction data using the Rietveld method,^{19,20} it is clear that the complex magnetic interactions in ThMn_{12} -type compounds are still best studied on single-crystal samples. Moreover, the most powerful techniques to study noncollinear magnetic structures such as zero-field neutron polarimetry require the use of single crystals.

It appears that YFe_4Al_8 and LuFe_4Al_8 do not melt congruently in stoichiometric proportions which may explain why crystals grown by Czochralski by pulling from a stoichiometric melt become enriched in Fe. Therefore large single crystals of YFe_4Al_8 and LuFe_4Al_8 for neutron-diffraction studies have to be grown by a different technique such as mineralization or flux growth.

ACKNOWLEDGMENTS

J. A. Paixão acknowledges financial support from JNICT under contract program PBIC/FIS/2213/95 and traveling funds from the Institute for Transuranium Elements-Joint Research Center of the European Commission. J. C. Waerenborgh acknowledges financial support from FCT under contract program PRAXIS/P/FIS/10040/1998.

- ¹H.-S. Li and J. M. D. Coey, *Handbook of Magnetic Materials* (North-Holland, Amsterdam, 1991), Vol. 6, p. 34.
- ²A. M. van der Kraan and K. H. J. Buschow, *Physica B* **86-88**, 93 (1977).
- ³K. H. J. Buschow and A. M. van der Kraan, *J. Phys. F: Met. Phys.* **8**, 921 (1978).
- ⁴I. Felner and I. Nowik, *J. Phys. Chem. Solids* **39**, 951 (1978).
- ⁵I. Felner, I. Nowik, K. Baberschke, and G. J. Nieuwenhuys, *Solid State Commun.* **44**, 691 (1982).
- ⁶I. Felner, I. Nowik, and M. Seh, *J. Magn. Magn. Mater.* **38**, 172 (1983).
- ⁷I. Felner and I. Nowik, *J. Magn. Magn. Mater.* **58**, 169 (1986).
- ⁸W. Schäfer, G. Will, G. M. Kalvius, and J. Gal, *Physica B* **156-157**, 751 (1989).
- ⁹J. Gal, I. Yaar, E. Arbaboff, H. Etedgi, F. J. Litterst, K. Aggarwal, J. A. Pereda, G. M. Kalvius, G. Will, and W. Schäfer, *Phys. Rev. B* **40**, 745 (1989).
- ¹⁰J. Gal, I. Yaar, D. Regev, S. Fredo, G. Shani, E. Arbaboff, W. Potzel, K. Aggarwal, J. A. Pereda, G. M. Kalvius, F. J. Litterst, W. Schäfer, and G. Will, *Phys. Rev. B* **42**, 8507 (1990).
- ¹¹A. Chelkowski, E. Talik, J. Szade, J. Heinmann, A. Winiarska, and A. Winiarski, *Physica B* **168**, 149 (1991).
- ¹²E. Talik, J. Szade, and J. Heinmann, *Physica B* **190**, 361 (1993).
- ¹³E. Talik, J. Heinmann, J. Szade, and T. Mydlarz, *Physica B* **205**, 127 (1995).
- ¹⁴A. P. Gonçalves, M. Almeida, C. T. Walker, J. Ray, and J. C. Spirlet, *Mater. Lett.* **19**, 13 (1994).
- ¹⁵J. A. Paixão, S. Langridge, S. Aa. Sørensen, B. Lebech, A. P. Gonçalves, G. H. Lander, P. J. Brown, P. Burlet, and E. Talik, *Physica B* **234-236**, 614 (1997).
- ¹⁶J. A. Paixão, B. Lebech, A. P. Gonçalves, P. J. Brown, G. H. Lander, P. Burlet, A. Delapalme, and J. C. Spirlet, *Phys. Rev. B* **55**, 14 370 (1997).
- ¹⁷J. A. Paixão, M. Ramos Silva, S. Aa. Sørensen, B. Lebech, G. H. Lander, P. J. Brown, S. Langridge, E. Talik, and A. P. Gonçalves, *Phys. Rev. B* **61**, 6176 (2000).
- ¹⁸S. Langridge, J. A. Paixão, N. Bernhoeft, C. Vettier, G. H. Lander, D. Gibbs, S. Aa. Sørensen, A. Stunault, D. Wermeille, and E. Talik, *Phys. Rev. Lett.* **82**, 2187 (1999).
- ¹⁹P. Schobinger-Papamantellos, K. H. J. Buschow, and C. Ritter, *J. Magn. Magn. Mater.* **186**, 21 (1997).
- ²⁰P. Schobinger-Papamantellos, K. H. J. Buschow, I. H. Hagmusa, F. R. de Boer, C. Ritter, and F. Fauth, *J. Magn. Magn. Mater.* **202**, 410 (1999).
- ²¹J. C. Waerenborgh, P. Salamakha, O. Sologub, A. P. Gonçalves, C. Cardoso, S. Serio, M. Godinho, and M. Almeida, *Chem. Mater.* **12**, 1743 (2000).
- ²²G. M. Sheldrick, SHELXL97, a program for the refinement of crystal structures, University of Göttingen, Germany, 1997.
- ²³J. A. Stone, appendix in G. M. Bancroft, A. G. Maddock, W. K. Ong, R. H. Prince, and J. A. Stone, *J. Chem. Soc. A* **1967**, 1966.
- ²⁴J. C. Waerenborgh, A. P. Gonçalves, and M. Almeida, *Solid State Commun.* **110**, 369 (1999).
- ²⁵P. J. Brown, J. B. Forsyth, and F. Tasset, *Proc. R. Soc. London, Ser. A* **442**, 147 (1993).
- ²⁶M. Blume, *Phys. Rev.* **130**, 1670 (1963).
- ²⁷P. J. Brown and J. C. Matthewman, *The Cambridge Crystallographic Subroutine Library-Mark 3 user's manual*, Rutherford Appleton Laboratory Report No. RAL-87-010, 1987 (unpublished).
- ²⁸K. Szymański, K. Recčko, L. Dobrzyński, and D. Satula, *J. Phys.: Condens. Matter* **11**, 6461 (1998).
- ²⁹J. A. Paixão, J. C. Waerenborgh, M. S. Rogalski, A. P. Gonçalves, M. Almeida, A. Gukasov, M. Bonnet, J. C. Spirlet, and J. B. Sousa, *J. Phys.: Condens. Matter* **40**, 4071 (1998).